

Cite this: DOI: 00.0000/xxxxxxxxxx

First-principles analysis of the optical properties of lead halide perovskite solution precursors

Giovanni Procida^a, Richard Schier^b, Ana M. Valencia^{a,b}, and Caterina Cocchi^{a,b,*}

Received Date

Accepted Date

DOI: 00.0000/xxxxxxxxxx

Lead halide perovskites are promising materials for optoelectronic and photovoltaic applications thanks to their favorable characteristics and low manufacturing costs. Characterizing the optical properties of their building blocks in different solvents is of great relevance to link the behavior of the solution precursors to the final thin films. Here, we focus on the charge-neutral solvated compounds with chemical formula, $\text{PbX}_2(\text{Sol})_4$, where X=Cl, Br, and I, and Sol are the six common solvent molecules $\text{C}_2\text{H}_3\text{N}$ (ACN), $\text{C}_3\text{H}_7\text{NO}$ (DMF), $\text{C}_2\text{H}_6\text{OS}$ (DMSO), $\text{C}_4\text{H}_6\text{O}_2$ (GBL), $\text{C}_5\text{H}_9\text{NO}$ (NMP). In the first-principles framework of time-dependent density-functional theory coupled to the polarizable continuum model, we investigate the electronic and optical properties of these systems. We find that both orbital energies and optical gaps are modulated by the presence of different halogen atoms as well as by the chemically bound solvent molecules. The latter, in particular, affect the energy and, to lesser extent, the spatial distribution of the molecular orbitals, thereby impacting on the character of the lowest-energy excitations. The presence of dark states at the absorption onset is generally promoted by electron-withdrawing solvents. Moreover, we find a clear correlation between the oscillator strength of the excitations and the relative contribution of the HOMO-LUMO transition, which remains optically active in all considered systems. Our results provide microscopic insight into the electronic and optical properties of lead halide perovskite solution precursors which is useful to unravel the evolution of these materials on their way to thin films.

1 Introduction

The power conversion efficiency of solar cells based on lead halide perovskites (LHP) has increased within a decade up to the current record of 29%.¹ Such an impressive performance is related to the intrinsic characteristics of these materials, including their large optical absorption coefficients, their high mobility, their long balanced carrier diffusion length, as well as their low exciton binding energies.^{2–8} These extraordinary opto-electronic properties are supported by the ability of LHPs to be synthesized by solution processing,^{9–16} which enables reduced production costs, high chemical tunability, and straightforward thin-film deposition.^{17–21} However, a critical aspect of this preparation method is that the nature of the solvents and their coupling with the solute may impact the characteristics of the final products.²² A number of recent studies addressing the stability of LHP solution precursors have confirmed that solute-solvent interactions influence the electronic and optical characteristics of the resulting thin-films.^{23–29} Additional works investigating intermediate phases have contributed to elucidate the key mechanisms ruling the formation of these materials and their evolution to the crystalline form.^{30–40}

Besides these important findings, a number of questions remain open regarding the electronic properties of LHP solution precursors and the microscopic understanding of their optical re-

sponse. While it is well established that actual samples contain various lead halide species with different charge and coordination numbers,^{23,27,38,41} including seed structures of iodoplumbate chains,⁴² the identification of their spectral signatures in solution as well as in subsequent (pseudo)crystalline stages of formation is very challenging, due to the manifold of coexisting structures and their non-trivial, mutual interactions.^{24,30,39,41,43} Given the intrinsic quantum-mechanical nature of the involved processes, experimental characterization only is insufficient to disentangle this intricate scenario.

Atomistic simulations have recently provided important insight into the formation of LHP solution precursors and their stability in different environments.^{27,28,44} However, there is still a lack of knowledge of the fundamental electronic interactions between lead and halogen atoms as well between solute and solvent species, which in turn determine the optical response of these complexes. This understanding is essential to complement experiments in the rationalization of the observed trends for excitation energies and oscillator strengths, in order to optimize the preparation of LHP solution precursors as well as to predict and interpret their evolution to efficient thin-films for photovoltaic and opto-electronic applications.

In first-principles work based on time-dependent density functional theory (TDDFT) coupled to the polarizable continuum model (PCM), we investigate the electronic and optical properties

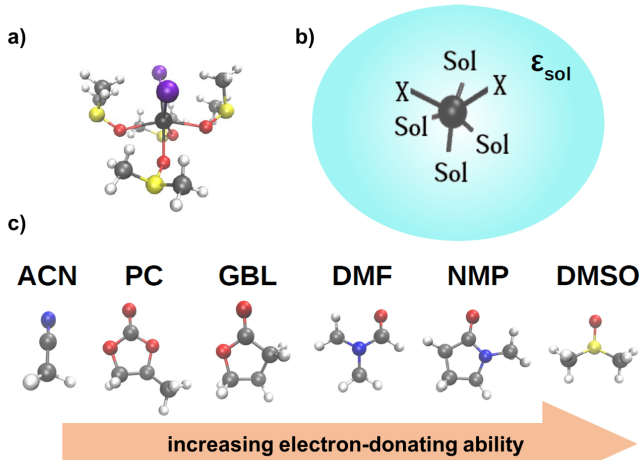


Fig. 1 a) Ball-and-stick representation of $\text{PbI}_2\text{DMSO}_4$ as exemplary compound investigated in this work; b) Pictorial sketch of $\text{PbX}_2(\text{Sol})$ complexes in a solvent cavity with dielectric function ϵ_{sol} ; c) Ball-and-stick representations of the solvent molecules considered in this work ordered from left to right according to their increasing electron-donating ability. C atoms are depicted in grey, H in white, O in red, N in blue, S in yellow, I in purple, and Pb in dark grey.

of a representative set of LHP solution precursors including the charge-neutral compounds with chemical formula PbX_2Sol_4 (see Fig. 1a and Fig. S1 in the ESI), where X = Cl, Br, I, and Sol stands for the six common solvent molecules $\text{C}_2\text{H}_3\text{N}$ (ACN), $\text{C}_3\text{H}_7\text{NO}$ (DMF), $\text{C}_2\text{H}_6\text{OS}$ (DMSO), $\text{C}_4\text{H}_6\text{O}_2$ (GBL), $\text{C}_5\text{H}_9\text{NO}$ (NMP). In the adopted *ab initio* formalism, where both quantum-mechanical as well as electrostatic solvent-solute interactions are accounted for, we are able to clarify how the considered solvent molecules chemically bound to the lead halide backbone affect the energies and the spatial distribution of the single-particle electronic states in the complexes. With this insight, we compute and analyze the optical absorption spectra, focusing specifically on the lowest-energy excitations, which, depending on the electron-donating activity of the solvent and its hybridization with the solute, can be optically active or almost dark, thereby influencing the photo-response of the LHP precursor.

2 Methodology

The results of this work are obtained from TDDFT⁴⁵ in the linear-response Casida scheme⁴⁶ coupled to the PCM⁴⁷ to account for the dielectric screening exerted by the solvent molecules onto the PbX_2 core. In the PCM framework, the solute is immersed in a homogeneous cavity in which the solvent is modelled implicitly by its dielectric constant, ϵ_{Sol} (see Fig. 1b).

The starting point of these calculations is the solution of the time-independent Kohn-Sham (KS) equations,⁴⁸ which, coupled to the PCM and in atomic units, read:

$$\left[\frac{1}{2} \nabla^2 + V_{\text{Hxc}}[\rho](\mathbf{r}) + V_{\text{ext}}(\mathbf{r}) + V_{\text{PCM}}[\rho](\mathbf{r}) \right] \phi_i^{\text{KS}}(\mathbf{r}) = \epsilon_i \phi_i^{\text{KS}}(\mathbf{r}), \quad (1)$$

where $\rho(\mathbf{r}) = \sum_{i=1}^N |\phi_i^{\text{KS}}(\mathbf{r})|^2$ is the electronic density generated by the N electrons in the system, and $\phi_i^{\text{KS}}(\mathbf{r})$ and ϵ_i the eigenfunc-

tion and eigenenergy of *i*-th KS state, respectively. In Eq. (1), three potential terms appear: $V_{\text{Hxc}}[\rho](\mathbf{r})$ is the combined Hartree exchange–correlation (Hxc) potential, which takes into account electron–electron interactions and needs to be approximated; $V_{\text{ext}}(\mathbf{r})$ is the external potential embedding the Coulomb attraction from the nuclei to the electrons; $V_{\text{PCM}}[\rho](\mathbf{r})$ is the effective potential describing the electrostatic interactions between solute and solvent.

To access excited-state properties, Eq. (1) has to be generalized to the time domain.⁴⁵ In the adopted linear-response formalism,⁴⁶ the problem is mapped into the eigenvalue equation, written below in compact matrix form as

$$\begin{pmatrix} A & B \\ B^* & A^* \end{pmatrix} \begin{pmatrix} X \\ Y \end{pmatrix} = \omega \begin{pmatrix} -1 & 0 \\ 0 & 1 \end{pmatrix} \begin{pmatrix} X \\ Y \end{pmatrix}, \quad (2)$$

where the eigenvalues ω_i are the excitation energies, and the eigenvectors, X_{ak}^i and Y_{ak}^i , are the resonant and antiresonant contributions, respectively, to the *i*-th excitation from the single-particle transitions between occupied (*k*) and unoccupied (*a*) states.

All calculations are performed with the code Gaussian 16.⁴⁹ Van der Waals interactions are accounted for through the semi-empirical Grimme D3 dispersion scheme.⁵⁰ In the structural optimizations, the cc-pVDZ basis set is employed for the light atoms (C, N, O, S, H) in conjunction with the LAN2DZ and LANL2 pseudopotentials and basis set for the heavy species (Pb, I, Br). The Perdew–Åkermark–Ernzerhof⁵¹ approximation for the exchange–correlation potential is adopted at this step. Geometries are relaxed until all interatomic forces are below 4×10^{-4} Ha/bohr. The following, tabulated values of dielectric functions of the considered solvent are employed within the PCM: $\epsilon_{\text{DMSO}}=46.7$, $\epsilon_{\text{DMF}}=38.2$, $\epsilon_{\text{ACN}}=36.6$, $\epsilon_{\text{NMP}}=32.5$, $\epsilon_{\text{GBL}}=41.7$, $\epsilon_{\text{PC}}=64.0$. The values for DMSO, DMF, and ACN are defined by default in Gaussian 16. The remaining references are taken from the literature.⁵² In the subsequent TDDFT calculations, the basis set for the light atoms is tightened in cc-pVTZ. The hybrid functional CAM-B3LYP⁵³ is employed at this step to approximate the exchange–correlation kernel.

We construct the considered 18 systems assuming an axial geometry for the PbX_2 backbone (see ESI, Fig. S1), which is known to be more stable than the equatorial arrangement.^{27,44} Four identical solvent molecules are bound to the Pb atom such that the resulting system is overall in a charge-neutral state. The solvent molecules considered in this work can be sorted according to their electron-donating ability,¹¹ as shown in Fig. 1c). ACN, which is the only solvent bound to Pb via a N atom, has the lowest electron-donating ability among the chosen ones. Conversely, DMSO, containing a S atom connecting the oxygen to methyl groups, has the highest tendency to donate electrons. In between, we find molecules that are bound to the PbX_2 backbone via an oxygen bridge.

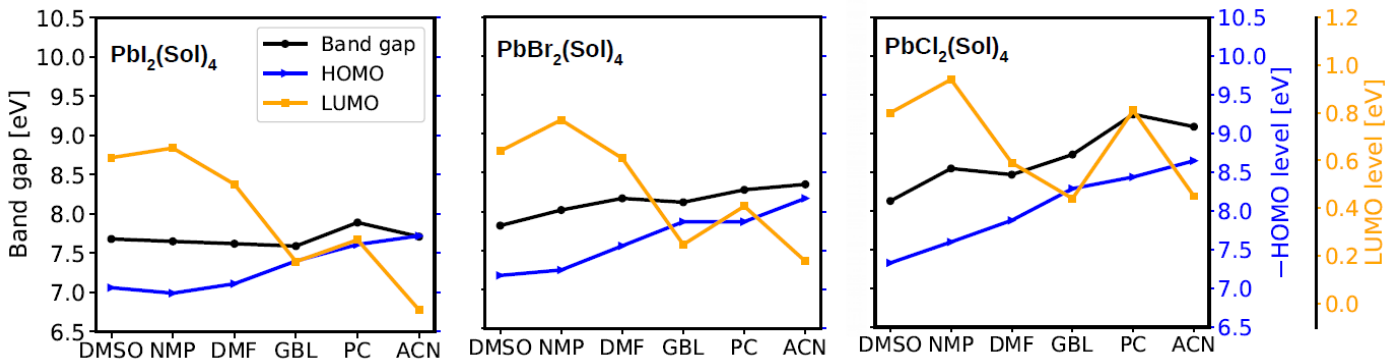


Fig. 2 Energies of -HOMO (blue triangles) LUMO (yellow square), as well as their absolute differences (band gaps, black circles) of the compounds considered in this work.

3 Results

3.1 Electronic properties

We start the analysis of the electronic properties of the considered compounds by examining the energies of their highest occupied molecular orbital (HOMO) and of the lowest unoccupied molecular orbital (LUMO). At a glance, the results reported in Fig. 2 are consistent with chemical intuition: the negative of the HOMO energy increases at decreasing size of the halogen atom while for the LUMO energies the opposite is generally true. These behaviors can be understood considering that the interaction of the lead-halide cores with electron-withdrawing solvent molecules leads to a stabilization of the HOMO energy, which becomes more negative thereby increasing its absolute value, and to a milder decrease of the LUMO energy (notice the different scales for the HOMO and LUMO energies in Fig. 2). An exception in this regard is given by the compounds containing PC, where the LUMO energy is always larger than expected from the trend.

The differences between HOMO and LUMO energies, plotted in Fig. 2 and labeled therein as “band gaps” for brevity, are obviously consistent with the picture described above: Larger values are obtained in the compounds with lighter halogen species and with solvent molecules with enhanced electron-withdrawing ability. Nonetheless, it is worth analyzing these results in more details, as their rationale is most relevant for the following discussion about optical properties. The variation of the band gaps with respect to the solvent molecules is much more pronounced in the PbCl₂-based compounds than in the others (see Fig. 2). This finding can be understood considering the backbone size. Solvent molecules chemically bound to PbCl₂ increase significantly the number of electrons in the systems. On the contrary, the large atomic size of iodine is such that the PbI₂ core alone contains 188 electrons. In this case, the contribution of the solvent molecules to the electronic cloud represents a small perturbation compared to the one of the inorganic backbone. Another relevant aspect is related to the influence of the electron-withdrawing character of the solvent molecules to the HOMO-LUMO gaps. In the presence of DMSO, which is the most electron-donating solvent among the considered ones, the HOMO-LUMO gap varies only within a few hundreds meV depending on the halogen species in the backbone. Conversely, the influence of the halogen species

is much more pronounced with PC and ACN, the most electron-withdrawing solvents in this study. This is consistent with their influence on the frontier orbital energies discussed above.

It is worth underlining that the values of the HOMO and LUMO energies reported in Fig. 2 should not be interpreted as excitation energies. In fact, in the context of DFT+PCM calculations, Koopman’s theorem is not expected to hold. The reason for this is the inability of the PCM to correctly capture the electronic reorganization occurring in the system upon ionization (see Ref. 54 for an extended discussion on this topic in the context of organic semiconductors). For this reason, the values of the -HOMO and LUMO energies plotted in Fig. 2 are quantitatively different from the ionization potentials (IP) and the electron affinities (EA) computed for reference within the ΔSCF method, as the difference between the total energies of the neutral species and its cation (IP) or anion (EA) and reported in the ESI, Fig. S2. Likewise, the HOMO-LUMO gaps differ substantially from the fundamental gaps calculated by subtracting for each system the corresponding EA from the IP (compare Fig. 2 and Fig. S2). This given, the qualitative agreement of the trends reported for the two sets of data with respect to the halide species and the solvent molecules confirms that the single-particle energies and their differences can be reliably used in the analysis of optical transitions (see Section 3.2). As a final remark, we notice that optical excitations computed from the TDDFT+PCM formalism do not suffer from the methodological issues discussed above for the single-particle energies. The reason behind it is that optical transitions leave the system in a charge-neutral configuration. To correctly describe this process, the non-equilibrium flavor of PCM⁵⁵ is adopted in the TDDFT calculations.

Before moving to the next part of our study, it is instructive to further extend our analysis to the energy levels in the close vicinity of the HOMO and the LUMO, plotted in Fig. 3. In most of the compounds considered in this work, the HOMO is energetically separated from the HOMO-1 by a few hundreds of meV, while the latter tends to be closer to the HOMO-2, with energy differences on the order of 100 meV. This behavior becomes more pronounced with decreasing size of the halogen atoms in the inorganic core. In all examined systems with PbCl₂ backbone, the HOMO is higher in energy than the HOMO-1 by at least 1 eV. On

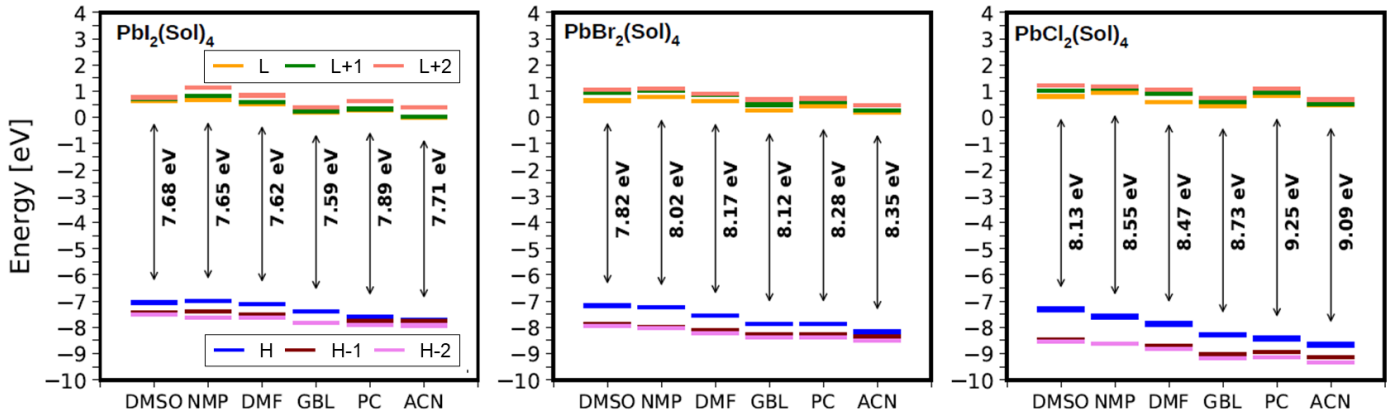


Fig. 3 Energy levels close to the frontier of the considered compounds. The values of the band gap are indicated.

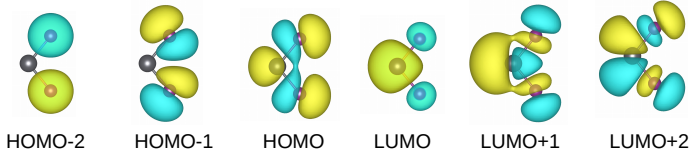


Fig. 4 Isosurfaces of the molecular orbitals computed for PbI_2 in an implicit solvent cavity.

the other hand, in both $\text{PbI}_2(\text{ACN})_4$, and $\text{PbBr}_2(\text{ACN})_4$, as well as in $\text{PbI}_2(\text{PC})_4$, the HOMO is energetically very close to both the HOMO-1 and the HOMO-2, with the energies of these states spanning a window of less than 400 meV. In the unoccupied region, the situation is more diversified, although, in general, the LUMO tends to be very close to the LUMO+1 and, in several cases, also to the LUMO+2, with these three states being separated from each other by a few hundreds of meV. Exceptions in this regard are given by $\text{PbI}_2(\text{NMP})_4$ and $\text{PbCl}_2(\text{DMF})_4$, where the LUMO+1 is above 1 eV in the absolute energy scale reported in Fig. 3, while the LUMO is at approximately 0.6 eV. All in all, from this analysis, it is evident that electron-withdrawing solvent molecules such as GBL, PC, and ACN tend to lower the HOMO energy, as a signature of electronic stabilization of the compounds induced by their interactions with the backbone. Conversely, electron-withdrawing solvents, such as DMSO, NMP, and DMF, lead to the opposite effect. These findings confirm the known trends for LHP solution precursors based on the coordination ability of the various solvents.^{11,27}

The spatial distributions of the molecular orbitals associated with the levels displayed in Fig. 3 preserve the characteristics of the corresponding wave-functions in the lead-halide backbone (see in Fig. 4 the orbitals of PbI_2 , which are visually identical to those of PbBr_2 and PbCl_2 , not shown). Specifically, the HOMO is formed by a combination of a p -state in the halogen atom and of the $6s$ state in Pb, while the HOMO-1 and the HOMO-2 include only contributions from halogen p -orbitals (no charge on Pb). In the unoccupied region, the first three molecular orbitals are dom-

inated by the hybridization of Pb and halogen p -states. In the solvated compounds, the chemical bond between the PbX_2 core and the solvent molecules⁴⁴ promotes charge delocalization to the latter (see Figs. S3 – S8 in the ESI). However, these electronic interactions act mainly on the energy of the states, as detailed in Fig. 3, rather than on the nature of the orbitals, as anticipated above. In terms of wave-function distribution, the most prominent effects of solute-solvent hybridization consist in a slight charge delocalization across the Pb-O bonds (or across the Pb-N bonds in ACN). Interestingly, these features are generally preserved in all systems, although the actual distribution of the orbitals depends on the details of solute-solvent hybridization and also on the size of the halide species (see Figs. S3 – S8). In general, these interactions tend to be more pronounced in the unoccupied levels and are more prominent in PbCl_2 -based compounds due to the smaller size of the Cl atom compared to the other considered halide species. With only 17 electrons distributed up to the $3s$ and $3p$ shells, the chemical environment provided by Cl to the Pb atom is not very different compared to the solvent molecules. As a result, the occupied electronic levels below the HOMO as well as the unoccupied ones become energetically close to each other, as discussed above with reference to Fig. 3, and the corresponding orbital distribution is more homogeneously spread over the entire compound.

3.2 Optical properties

We start the analysis of the optical properties from the computed absorption spectra. We focus specifically on the lead-halide compounds interacting with the most electron-donating solvent (DMSO), the most electron-withdrawing one (ACN), as well as GBL, which sets itself between the former two (see Fig. 1a). The optical spectra of these systems are plotted in Fig. 5, while those of the remaining compounds are reported in the ESI, Fig. S9. From the trends depicted in Figs. 2 and 3, it is reasonable to expect that the absorption onset increases in energy with decreasing size of the halogen atoms, while it decreases with increasing electron-donating ability of the solvent molecules. The results shown in Fig. 5 are only partly consistent with this intuition.

The spectra of the compounds with PbBr_2 and PbI_2 backbones

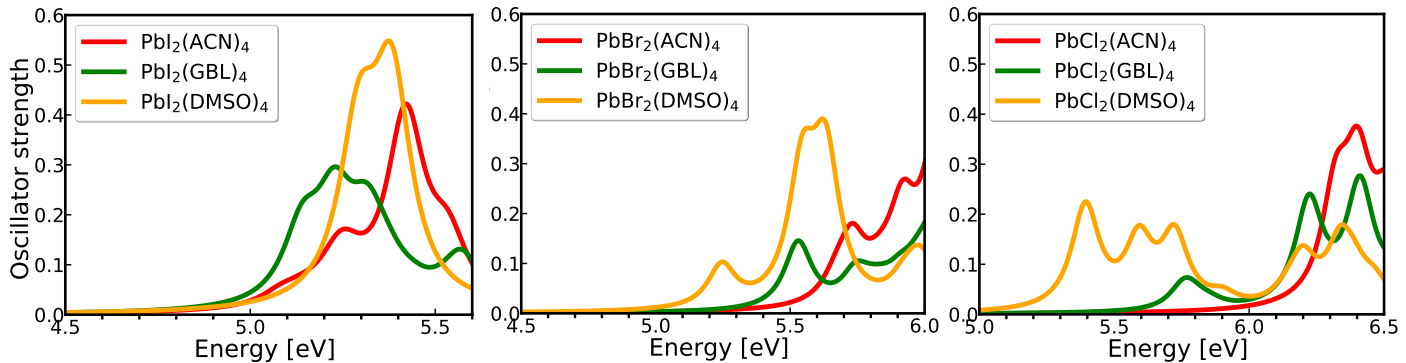


Fig. 5 Optical absorption spectra of $\text{PbX}_2(\text{DMSO})_4$, $\text{PbX}_2(\text{GBL})_4$, and $\text{PbX}_2(\text{ACN})_4$ with $\text{X} = \text{I}$ (left), $\text{X} = \text{Br}$ (middle), $\text{X} = \text{Cl}$ (right). A Lorentzian broadening of 125 meV is applied to all spectra.

exhibit the first peaks at higher energies compared to their PbCl_2 -based counterparts (notice the different energy scales in the three panels of Fig. 5). The increasing electron-donating ability of the solvents is reflected in the red-shift of the absorption onsets, as expected based on the results in Figs. 2 and 3. However, in the spectra of the $\text{PbX}_2(\text{DMSO})_4$ compounds, the absorption onset undergoes a red-shift of ~ 200 meV upon decreasing size of the halogen species, consistent with the results obtained for the electronic gaps (Fig. 2). In the spectra of the PbI_2 -based systems (Fig. 5, left panel), the lowest-energy onset corresponding to the compound in GBL is in line with the trends of the HOMO-LUMO gaps (Figs. 2 and 3), although in absolute terms the difference between the absorption onset energies is larger compared to the band gap energies. This discrepancy can be explained recalling the issues with the quantitative interpretation of the single-particle energies calculated within the DFT+PCM formalism (see end of Section 3.1 and Ref. 54). The qualitative agreement between the two sets of data is therefore satisfactory.

To gain further insight into the optical properties, we analyze more closely their lowest-energy excitations. A visual overview is provided in Fig. 6, top panel, for all systems investigated in this work, while all details are reported in the ESI, Tables S1 – S18. In the PbI_2 -based compounds, the energies of first excitations are comprised within a window of less than 300 meV, while in the systems with PbBr_2 , backbone they cover a twice as large energy range; finally, in the chlorinated materials, the energies of the first excited states vary within approximately 1 eV. This trend is consistent with the energy distribution of the HOMO-LUMO gaps (Fig. 2) and can be explained analogously (see Section 3.1): Solvent molecules bound to the PbCl_2 -based compounds increase the number of electrons more dramatically than with the PbI_2 cores, thereby affecting more prominently the distribution of the single-particle states and hence the transition energies between them. Yet, excitation energies are *per se* insufficient to rationalize optical spectra: the oscillator strengths (OS) of the excited states and their composition in terms of single-particle transitions provide valuable information too.

Focusing on the $\text{PbI}_2(\text{Sol})_4$ compounds first (Fig. 6, top left panel), we notice that the system bound to DMF exhibits the most intense first excitation; in the case of $\text{PbI}_2(\text{DMSO})_4$ and

$\text{PbI}_2(\text{GBL})_4$, the oscillator strength of the lowest-energy peak is lower than in $\text{PbI}_2(\text{DMF})_4$ but still non-negligible; finally, in $\text{PbI}_2(\text{NMP})_4$, $\text{PbI}_2(\text{PC})_4$, and especially $\text{PbI}_2(\text{ACN})_4$, the first excitation can be considered almost dark, having an OS below 0.1 (see ESI for the corresponding values). The reason for the different OS exhibited by the first excitation of these compounds can be traced back to their composition in terms of single-particle transitions. By inspecting once again the molecular orbitals shown in Fig. 4, it is clear that transitions from the HOMO to the LUMO are optically allowed, due to the *s*- and *p*-character of the contributions localized on the Pb atom in the respective wave-function distributions; this characteristic is preserved also in the presence of the solvent molecules (see Figs. S3 – S8 in the ESI). For this reason, we analyze the relative weight of the HOMO \rightarrow LUMO transition to the lowest-energy excitation in each considered system.

From the corresponding plots, shown on the bottom panel of Fig. 6, the off-trend behavior exhibited by $\text{PbI}_2(\text{ACN})_4$, $\text{PbI}_2(\text{PC})_4$, $\text{PbBr}_2(\text{ACN})_4$, and $\text{PbCl}_2(\text{GBL})_4$ is clearly noticeable: in all these systems, the first excitation receives a low or negligible contribution from the HOMO \rightarrow LUMO transition, and the OS is well below 0.1 (see Tables S1, S2, S7, S15). This behavior can be understood considering the electronic structure of these compounds. Going back to Fig. 3, we notice that in $\text{PbI}_2(\text{ACN})_4$, in $\text{PbI}_2(\text{PC})_4$, and in $\text{PbBr}_2(\text{ACN})_4$, both frontier orbitals are very close to the neighboring energy levels, while for $\text{PbCl}_2(\text{GBL})_4$ this is true for the LUMO only. As a result, several single-particle transitions contribute to the first excited state, with a predominance of HOMO-1 \rightarrow LUMO in $\text{PbI}_2(\text{ACN})_4$, $\text{PbI}_2(\text{PC})_4$ and in $\text{PbBr}_2(\text{ACN})_4$. In the case of $\text{PbCl}_2(\text{GBL})_4$, the situation is even more complex, as more than five transitions all with weights below 15% contribute to the first excitation. Based on the distribution of the HOMO-1 and of the LUMO in the lead halide backbone (see Fig. 4) their transition is expected to be optically inactive (see also Tables S19 – S21 in the ESI). The interaction with the solvent molecules promotes charge delocalization onto the latter and breaks the symmetry of the inorganic core: as a result, the OS in these systems is almost one order of magnitude larger than in the isolated PbX_2 units. Nonetheless, it is clear from Fig. 5 (and Fig. S2 for $\text{PbI}_2(\text{PC})_4$) that the first excitation does not contribute substantially to the optical absorption of these systems. As a side note, we mention

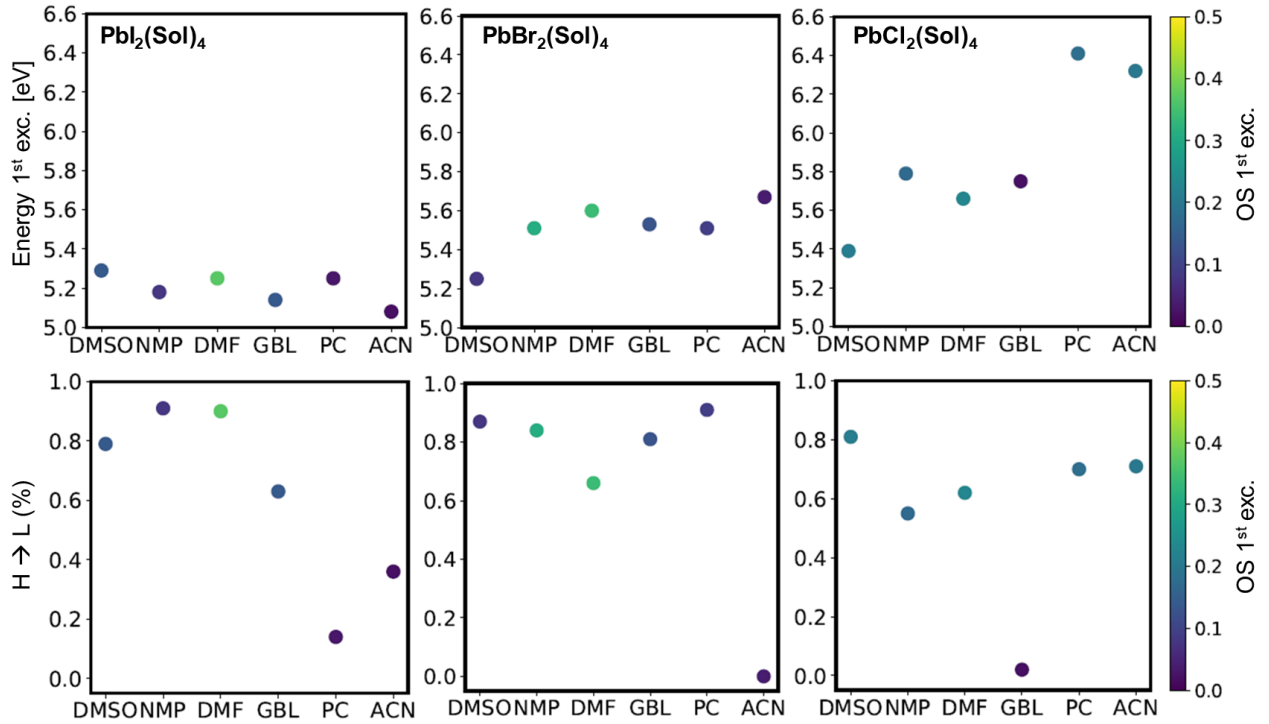


Fig. 6 Analysis of the first excitation in all the considered systems, from left to right, $\text{PbI}_2(\text{Sol})_4$, $\text{PbBr}_2(\text{Sol})_4$, and $\text{PbCl}_2(\text{Sol})_4$. Top: Excitation energy; Bottom: Fractional amount of the HOMO \rightarrow LUMO transitions contributing to the first excitation. The color bar indicates the oscillator strength (OS).

that the same behavior for $\text{PbI}_2(\text{PC})_4$ is reproduced by many-body perturbation theory (MBPT) calculations *in vacuo* (see Table S22 in the ESI). In the case of $\text{PbI}_2(\text{ACN})_4$, MBPT predicts the first excitation to stem almost entirely from the HOMO \rightarrow LUMO transition. However, in this compound, the quasi-particle correction to the orbital energies computed from G_0W_0 switches the order for the HOMO and HOMO-1 (see Fig. S11), such that, effectively, the first excitation in both $\text{PbI}_2(\text{PC})_4$ and $\text{PbI}_2(\text{ACN})_4$ is dominated by the same orbital transition.

Inspecting now the other results plotted in Fig. 6, bottom panel, we notice that in all compounds except those discussed above, the weight of the HOMO \rightarrow LUMO transition to the first excitation is above 50% and, correspondingly, the OS is close to or above 0.1 (see ESI for details). Indeed, there is a clear correlation between the OS and the contribution of the transition between the frontier orbitals. The most remarkable example is given by the compounds interacting with DMF: in all these three systems, the first excitation has an oscillator strength above 0.25 and a relative HOMO \rightarrow LUMO weight larger than 60%.

From the analysis of the optical properties for the PbX_2 compounds computed in an implicit solvent cavity but without explicit solvent molecules, we find that the behaviors rationalized above stem directly from the electronic and optical properties of the lead halide backbones. As detailed in the ESI, on Tables S19 – S21, also in these systems the lowest-energy excitation is bright, as visible in the optical spectra (Fig. S10), and it is almost entirely given by the HOMO \rightarrow LUMO transition. However, in the absence of chemically bound solvent molecules, the associated OS is only

of the order of 10^{-2} , suggesting that the presence of the latter actually enhances the optical activity of this transition. The most intense excitation is associated with the HOMO \rightarrow LUMO + 1, which gives rise to the strong peak, which is found at least 1.5 eV above the onset depending on the halogen species. The relatively large OS associated with the HOMO \rightarrow LUMO + 1 transition is present also in the explicitly solvated compounds. In most cases, it also appears at higher energies compared to the first bright excitation, such that it does enter the range plotted in Figs. 5 and S9 (see Tables S1 – S18 for details). However, due to the higher density of excited states in the $\text{PbX}_2(\text{Sol})_4$ compounds compared to the PbX_2 ones, the energy differences between the excitations dominated by the HOMO \rightarrow LUMO and the HOMO \rightarrow LUMO + 1 transitions are within 1 eV. There are nonetheless some exceptions to this behavior, with the most significant one concerning the systems interacting with DMSO. Regardless of the halogen atom in the backbone, in these compounds, the second excitation is dominated by the HOMO \rightarrow LUMO + 1 contribution and it is therefore as intense as the first one in the spectra of $\text{PbI}_2(\text{DMSO})_4$ and $\text{PbCl}_2(\text{DMSO})_4$, and even more intense in the spectrum of $\text{PbBr}_2(\text{DMSO})_4$ (see Fig. 5).

For further comparison, we comment now on the optical spectra computed for the PbI_2 -based compounds in the framework of MBPT^{56–58} without the inclusion of implicit solvation effects. The same approach was successfully applied in Ref. 42 in comparison with experimental data. The trends provided by these results (see ESI, Fig. S9, S10, and Table S19) are consistent with those obtained from TDDFT+PCM: larger electronic and optical gaps are

associated with compounds with electron-donating groups. We notice, however, that the absolute values of the excitation energies computed from MBPT are systematically lower compared to those in Fig. 5 (see Fig. S12). This can be explained considering that the quasi-particle correction included via the G_0W_0 approximation on top of the DFT results (CAM-B3LYP functional) increases the band-gap size. On top of this, the electron-hole interaction explicitly accounted for in the solution of the Bethe-Salpeter equation red-shifts the absorption onset by more than 3.5 eV in each system. This value, which is interpreted as the exciton binding energy, is of the typical order of magnitude of small molecules^{59,60}

Optical absorption spectra measured for lead iodide perovskite precursors in different solvents are in overall agreement with our findings.³⁸ It is important to recall that in actual samples, different species coexist and contribute to the detected optical absorption spectra.^{23,27,38,42} Nonetheless, we can comment qualitatively on the fingerprints associated to the neutral $\text{PbI}_2(\text{Sol})_4$ species therein. In the measurements reported in Ref. 38, the peak energies assigned to the lowest-energy transitions in $\text{PbI}_2(\text{GBL})_4$, $\text{PbI}_2(\text{DMSO})_4$, $\text{PbI}_2(\text{NMP})_4$, and $\text{PbI}_2(\text{DMF})_4$ are almost at the same energy, which is not in contrast with our findings, considering the inhomogeneous broadening in the experimental spectra. Interestingly, in the same work, the peak associated to the $\text{PbI}_2(\text{DMSO})_4$ species is much more intense than its counterpart for $\text{PbI}_2(\text{GBL})_4$,³⁸ in qualitative agreement with our results shown in Fig. 5, left panel. Even in Ref. 27, a lower absorption onset of $\text{PbI}_2(\text{GBL})_4$ compared to $\text{PbI}_2(\text{DMSO})_4$ is reported for measurements of these compounds in the presence of the methylammonium cation. The systematic blue-shift of our computed spectra with respect to experimental references is to be mainly ascribed to the absence in our calculations of the non-negligible contributions of spin-orbit coupling⁶¹ and to the absence of additional intermolecular interactions beyond those between the PbX_2 backbones and the nearest-neighboring solvent molecules. However, as demonstrated in Ref. 42, a quantitative misalignment with experimental absorption energies does not affect the insight provided by theory in the interpretation of the measured spectra.

3.3 Summary and Conclusions

In summary, we have presented a first-principles study of the electronic and optical properties of a representative set of charge-neutral LHP solution precursors with chemical formula $\text{PbX}_2(\text{Sol})_4$ ($\text{Sol} = \text{DMSO}$, PC, NMP, DMF, GBL, and ACN). Our analysis reveals the correlation between the electron-donating ability of the solvent molecules and the decreasing size of the band gap of the solutes, due to a concomitant decrease (increase) of the HOMO (LUMO) energy. Notably, this trend is highly sensitive of the halogen atoms in the backbone: in the presence of iodine, band gaps span an energy window of less than 0.5 eV; when the solute contains Br and especially Cl, the band-gap values of the investigated systems vary within a range of approximately 1 eV. Orbital hybridization between solute species and explicit solvent molecules occur mainly in the unoccupied region

and is more prominent in the PbCl_2 -based compounds due to the smaller number of electrons in chlorine atoms compared to the other considered halogen species. However, these effects do not alter the nature of the molecular orbitals, which preserve their character as in the lead halide backbone. The inclusion of heavier halogen atoms in the inorganic core leads to a redshift of the absorption onset, in accordance with the aforementioned trends of the HOMO-LUMO gaps. Except for a few compounds with electron-withdrawing solvents such as $\text{PbI}_2(\text{PC})_4$, $\text{PbI}_2(\text{ACN})_4$, $\text{PbBr}_2(\text{ACN})_4$, and $\text{PbCl}_2(\text{GBL})_4$, in all systems, the lowest-energy excitation is bright and corresponds to the optically active $\text{HOMO}\rightarrow\text{LUMO}$ transition. The correlation between the weight of this contribution to the first excited state and the oscillator strength of the latter is key to understand the optical absorption of these compounds.

In conclusion, with this study, we have clarified the fundamental relations between absorption spectra and electronic structure of LHP solution precursors, and highlighted how the halogen atoms in the inorganic core as well as the solvent molecules can critically impact the optical response of these compounds. Our findings are useful to identify and interpret the fingerprints of the neutral species $\text{PbX}_2(\text{Sol})_2$ in optical absorption measurements, where the contributions of these compounds are entangled with those of lead halide species with different coordination numbers that coexist in the samples. The disclosed non-trivial effects of the solvent molecules on the single-particle levels close to the frontier suggest that a simplistic interpretation of the optical absorption based solely on the molecular orbital trends is insufficient to interpret the spectra of LHP solution precursors. While the optically-active $\text{HOMO}\rightarrow\text{LUMO}$ transition is often dominating the first excitation, in the cases when this is not true the insight provided by our study can be of great help. The theoretical framework adopted herein and the presented analysis can be successfully extended also to other lead halide species that are detected in the samples, as well as to LHP intermediate structures identified at subsequent stage of formation. As such, the outcomes of this study provide a valuable starting point to better understand the role solute-solvent interactions in the evolution of LHPs on their way to crystalline thin films.

Conflicts of interest

There are no conflicts to declare.

Acknowledgements

We are grateful to Jannis Krumland, Michele Guerrini, Oleksandra Shargaieva, and Eva Unger for fruitful discussions. This work was supported by the German Research Foundation (DFG), Priority Programm SPP 2196 - Project number 424394788, by the German Federal Ministry of Education and Research (Professorinnenprogramm III), and from the State of Lower Saxony (Professorinnen fÃ¼r Niedersachsen). Calculations were performed on the HPC cluster CARL at the University of Oldenburg, funded by the DFG (Project No. INST 184/157-1 FUGG) and by the Ministry of Science and Culture of the State of Lower Saxony.

Notes and references

- 1 A. Al-Ashouri, E. Köhnen, B. Li, A. Magomedov, H. Hempel, P. Caprioglio, J. A. Márquez, A. B. M. Vilches, E. Kasparavicius, J. A. Smith, N. Phung, D. Menzel, M. Grischeck, L. Kegelmann, D. Skroblin, C. Gollwitzer, T. Malinauskas, M. Jost, G. Matic, B. Rech, M. Schlatmann, Rutger abd Topic, L. Korte, A. Abate, B. Stanowski, D. Neher, M. Stolterfoht, T. Unold, V. Getautis and S. Albrecht, *Science*, 2020, **370**, 1300–1309.
- 2 S. D. Stranks, G. E. Eperon, G. Grancini, C. Menelaou, M. J. Alcocer, T. Leijtens, L. M. Herz, A. Petrozza and H. J. Snaith, *Science*, 2013, **342**, 341–344.
- 3 V. D'Alessandro, G. Grancini, M. J. Alcocer, A. R. S. Kandada, S. D. Stranks, M. M. Lee, G. Lanzani, H. J. Snaith and A. Petrozza, *Nature Comm.*, 2014, **5**, 1–6.
- 4 A. E. Shalan, T. Oshikiri, S. Narra, M. M. Elshanawany, K. Ueno, H.-P. Wu, K. Nakamura, X. Shi, E. W.-G. Diau and H. Misawa, *ACS Appl. Mater. Interfaces*, 2016, **8**, 33592–33600.
- 5 Z. Xiao and Y. Yan, *Adv. Energy Mater.*, 2017, **7**, 1701136.
- 6 Z. Yang, A. Surrete, K. Galkowski, N. Bruyant, D. K. Maude, A. A. Haghimirad, H. J. Snaith, P. Plochocka and R. J. Nicholas, *J. Phys. Chem. Lett.*, 2017, **8**, 1851–1855.
- 7 P. Umari, E. Mosconi and F. De Angelis, *J. Phys. Chem. Lett.*, 2018, **9**, 620–627.
- 8 J. Lim, M. T. Hörtner, N. Sakai, J. M. Ball, S. Mahesh, N. K. Noel, Y.-H. Lin, J. B. Patel, D. P. McMeekin, M. B. Johnston, B. Wenger and H. J. Snaith, *Energy Environ. Sci.*, 2019, **12**, 169–176.
- 9 S.-G. Li, K.-J. Jiang, M.-J. Su, X.-P. Cui, J.-H. Huang, Q.-Q. Zhang, X.-Q. Zhou, L.-M. Yang and Y.-L. Song, *J. Mater. Chem. A*, 2015, **3**, 9092–9097.
- 10 Z. Yang, C.-C. Chueh, F. Zuo, J. H. Kim, P.-W. Liang and A. K.-Y. Jen, *Adv. Energy Mater.*, 2015, **5**, 1500328.
- 11 J. C. Hamill Jr, J. Schwartz and Y.-L. Loo, *ACS Energy Lett.*, 2017, **3**, 92–97.
- 12 C. McDowell, M. Abdelsamie, M. F. Toney and G. C. Bazan, *Adv. Mater.*, 2018, **30**, 1707114.
- 13 M. Jung, S.-G. Ji, G. Kim and S. I. Seok, *Chem. Soc. Rev.*, 2019, **48**, 2011–2038.
- 14 T. Soto-Montero, W. Soltanpoor and M. Morales-Masis, *APL Mater.*, 2020, **8**, 110903.
- 15 J. Kim, B.-w. Park, J. Baek, J. S. Yun, H.-W. Kwon, J. Seidel, H. Min, S. Coelho, S. Lim, S. Huang, K. Gaus, M. A. Green, T. J. Shin, A. W. Y. Ho-baillie, M. G. Kim and S. I. Seok, *J. Am. Chem. Soc.*, 2020, **142**, 6251–6260.
- 16 B. Zhou, D. Ding, Y. Wang, S. Fang, Z. Liu, J. Tang, H. Li, H. Zhong, B. Tian and Y. Shi, *Adv. Opt. Mater.*, 2021, **9**, 2001435.
- 17 N. J. Jeon, J. H. Noh, Y. C. Kim, W. S. Yang, S. Ryu and S. I. Seok, *Nature Mat.*, 2014, **13**, 897–903.
- 18 Y. Wu, A. Islam, X. Yang, C. Qin, J. Liu, K. Zhang, W. Peng and L. Han, *Energy Environ. Sci.*, 2014, **7**, 2934–2938.
- 19 T. Zhang, N. Guo, G. Li, X. Qian, L. Li and Y. Zhao, *J. Mater. Chem. A*, 2016, **4**, 3245–3248.
- 20 B. Daenekamp, C. Müller, M. Sendner, P. P. Boix, M. Sessolo, R. Lovrincic and H. J. Bolink, *J. Phys. C*, 2018, **9**, 2770–2775.
- 21 D. Huang, P. Xie, Z. Pan, H. Rao and X. Zhong, *J. Mater. Chem. A*, 2019, **7**, 22420–22428.
- 22 Y. Vaynzof, *Advanced Energy Materials*, 2020, **10**, 2003073.
- 23 S. Rahimnejad, A. Kovalenko, S. M. Forés, C. Aranda and A. Guerrero, *Chem. Phys. Chem.*, 2016, **17**, 2795–2798.
- 24 S. J. Yoon, K. G. Stamplecoskie and P. V. Kamat, *J. Phys. Chem. Lett.*, 2016, **7**, 1368–1373.
- 25 J. Stevenson, B. Sorenson, V. H. Subramaniam, J. Raiford, P. P. Khlyabich, Y.-L. Loo and P. Clancy, *Chem. Mater.*, 2017, **29**, 2435–2444.
- 26 A. Shareiko, C. Mackeen, L. Jewell, F. Bridges and M. F. Toney, *Chem. Mater.*, 2017, **29**, 1315–1320.
- 27 E. Radicchi, E. Mosconi, F. Elisei, F. Nunzi and F. De Angelis, *ACS Appl. Energy Mater.*, 2019, **2**, 3400–3409.
- 28 E. Radicchi, A. Kachmar, E. Mosconi, B. Bizzarri, F. Nunzi and F. De Angelis, *J. Phys. Chem. Lett.*, 2020, **11**, 6139–6145.
- 29 B. A. Sorenson, L. U. Yoon, E. Holmgren, J. J. Choi and P. Clancy, *J. Mater. Chem. A*, 2021, **9**, 3668–3676.
- 30 J. S. Manser, B. Reid and P. V. Kamat, *J. Phys. Chem. C*, 2015, **119**, 17065–17073.
- 31 Y. Guo, K. Shoyama, W. Sato, Y. Matsuo, K. Inoue, K. Harano, C. Liu, H. Tanaka and E. Nakamura, *J. Am. Chem. Soc.*, 2015, **137**, 15907–15914.
- 32 J. Cao, X. Jing, J. Yan, C. Hu, R. Chen, J. Yin, J. Li and N. Zheng, *J. Am. Chem. Soc.*, 2016, **138**, 9919–9926.
- 33 A. A. Petrov, I. P. Sokolova, N. A. Belich, G. S. Peters, P. V. Dorovatovskii, Y. V. Zubavichus, V. N. Khrustalev, A. V. Petrov, M. Grădățel, E. A. Goodilin and A. B. Tarasov, *J. Phys. Chem. C*, 2017, **121**, 20739–20743.
- 34 B. J. Foley, J. Girard, B. A. Sorenson, A. Z. Chen, J. S. Niezgoda, M. R. Alpert, A. F. Harper, D.-M. Smilgies, P. Clancy, W. A. Saidi and J. J. Choi, *J. Mater. Chem. A*, 2017, **5**, 113–123.
- 35 Y. Li, L. Zhi, G. Ge, Z. Zhao, X. Cao, F. Chen, X. Cui, F. Lin, L. Ci, J. Sun, D. Zhuang and J. Wei, *Cryst. Growth Des.*, 2018, **19**, 959–965.
- 36 S. A. Fateev, A. A. Petrov, V. N. Khrustalev, P. V. Dorovatovskii, Y. V. Zubavichus, E. A. Goodilin and A. B. Tarasov, *Chem. Mater.*, 2018, **30**, 5237–5244.
- 37 B. Li, D. Binks, G. Cao and J. Tian, *Small*, 2019, **15**, 1903613.
- 38 O. Shargaieva, H. Näsström, J. A. Smith, D. Többens, R. Munir and E. Unger, *Mater. Adv.*, 2020, **1**, 3314–3321.
- 39 M. Vásquez-Montoya, J. F. Montoya, D. Ramirez and F. Jaramillo, *J. Energy Chem.*, 2021, **57**, 386–391.
- 40 W. Kaiser, E. Mosconi, A. A. Alothman, D. Meggiolaro, A. Gagliardi and F. De Angelis, *Mater. Adv.*, 2021.
- 41 O. Shargaieva, L. Kuske, J. Rappich, E. Unger and N. H. Nickel, *ChemPhysChem*, 2020, **21**, 2327.
- 42 A. M. Valencia, O. Shargaieva, R. Schier, E. Unger and C. Cocchi, *J. Phys. Chem. Lett.*, 2021, **12**, 2299–2305.
- 43 T. Yu, L. Zhang, J. Shen, Y. Fu and Y. Fu, *Dalton Trans.*, 2014, **43**, 13115–13121.
- 44 R. Schier, A. Comes Rodríguez, A. M. Valencia and C. Cocchi, *arXiv preprint arXiv:2107.04307*, 2021.
- 45 E. Runge and E. K. Gross, *Phys. Rev. Lett.*, 1984, **52**, 997.
- 46 M. E. Casida and M. Huix-Rotllant, *Annu. Rev. Phys. Chem.*, 2012, **63**, 287–323.
- 47 J. Tomasi, B. Mennucci and R. Cammi, *Chem. Rev.*, 2005, **105**, 2999–3094.
- 48 W. Kohn and L. J. Sham, *Phys. Rev.*, 1965, **140**, A1133–A1138.
- 49 M. J. Frisch, G. W. Trucks, H. B. Schlegel, G. E. Scuseria, M. A. Robb, J. R. Cheeseman, G. Scalmani, V. Barone, G. A. Petersson, H. Nakatsuji, X. Li, M. Caricato, A. V. Marenich, J. Bloino, B. G. Janesko, R. Gomperts, B. Mennucci, H. P. Hratchian, J. V. Ortiz, A. F. Izmaylov, J. L. Sonnenberg, D. Williams-Young, F. Ding, F. Lipparini, F. Egidi, J. Goings, B. Peng, A. Petrone, T. Henderson, D. Ranasinghe, V. G. Zakrzewski, J. Gao, N. Rega, G. Zheng, W. Liang, M. Hada, M. Ehara, K. Toyota, R. Fukuda, J. Hasegawa, M. Ishida, T. Nakajima, Y. Honda, O. Kitao, H. Nakai, T. Vreven, K. Throssell, J. A. Montgomery, Jr., J. E. Peralta, F. Ogliaro, M. J. Bearpark, J. J. Heyd, E. N. Brothers, K. N. Kudin, V. N. Staroverov, T. A. Keith, R. Kobayashi, J. Normand, K. Ragahavachari, A. P. Ryndell, J. C. Burant, S. S. Iyengar, J. Tomasi, M. Cossi, J. M. Millam, M. Klene, C. Adamo, R. Cammi, J. W. Ochterski, R. L. Martin, K. Morokuma, O. Farkas, J. B. Foresman and D. J. Fox, *Gaussian 16 Revision A.03*, 2016, Gaussian Inc. Wallingford CT.
- 50 S. Grimme, J. Antony, S. Ehrlich and H. Krieg, *J. Chem. Phys.*, 2010, **132**, 154104.
- 51 J. P. Perdew, K. Burke and M. Ernzerhof, *Phys. Rev. Lett.*, 1996, **77**, 3865–3868.
- 52 C. Wohlfarth, *Static Dielectric Constants of Pure Liquids and Binary Liquid Mixtures: Supplement to Volume IV/17 (Landolt-Bornstein: Numerical Data and Functional Relationships in Science and Technology—New Series)*, 2015.
- 53 T. Yanai, D. P. Tew and N. C. Handy, *Chem. Phys. Lett.*, 2004, **393**, 51–57.
- 54 J. Krumland, A. M. Valencia and C. Cocchi, *Phys. Chem. Chem. Phys.*, 2021, **23**, 4841–4855.
- 55 R. Cammi and J. Tomasi, *Int. J. Quantum Chem.*, 1995, **56**, 465–474.
- 56 F. Weigend, A. Köhn and C. Hättig, *J. Chem. Phys.*, 2002, **116**, 3175–3183.
- 57 F. Bruneval, *J. Chem. Phys.*, 2012, **136**, 194107.
- 58 F. Bruneval, T. Rangel, S. M. Hamed, M. Shao, C. Yang and J. B. Neaton, *Comput. Phys. Commun.*, 2016, **208**, 149–161.
- 59 D. Hirose, Y. Noguchi and O. Sugino, *Phys. Rev. B*, 2015, **91**, 205111.
- 60 C. Cocchi and C. Draxl, *Phys. Rev. B*, 2015, **92**, 205126.
- 61 C. Borghesi, E. Radicchi, L. Belpassi, D. Meggiolaro, F. De Angelis and F. Nunzi, *Comput. Theor. Chem.*, 2019, **1164**, 112558.